Referência
FERRARI, J. M.; KAYSER, F.; GOULART, J. N. V. Numerical prediction of local convective heat transfer and skin friction in eccentric annulus tube. In: INTERNATIONAL CONFERENCE ON HEAT TRANSFER, FLUID MECHANICS AND THERMODYNAMICS (HEFAT), 15th., 2021, Virtual.

NUMERICAL PREDICTION OF LOCAL CONVECTIVE HEAT TRANSFER AND SKIN FRICTION IN ECCENTRIC ANNULUS TUBE

Ferrari J.M.S.*, Kayser F.M. and Goulart J.N.V.
*Author for correspondence
Experimental and Computational Mechanics Group - GMEC,
University of Brasília,
Brasília, 72444-240,
Brazil,
E-mail: jalusaferrari@gmail.com

ABSTRACT

Non-isothermal turbulent flow was investigated in both concentric and eccentric annulus under the same thermal boundary conditions, using RANS and URANS/LES turbulence hybrid mode. Inlet temperature was prescribed at the entrance and constant wall heat flux, q" = 1000 [W/m²], was imposed on the inner's tube surface, while the outer wall was kept adiabatic. The annulus geometric parameters inner (*d*), outer (*D*) diameters and length (*L*) were kept unchanged throughout the computations, yielding *d/D*-ratio and L/D_h, 0.494 and 58.36, respectively. Two different eccentricities were simulated, e = 0 (concentric case) and 0.8. Stationary and time-dependent simulations were run for eccentric annulus, whereas for the concentric one only stationary solution was obtained. Transient runs in eccentric annulus of 0.8 showed periodic flow patterns producing high crossing velocity components and temperature fluctuations through the narrow gap. Further, such fluctuations also improved the quality of the convective heat transfer, lowering the inner wall temperature, mainly near the narrow gap. At the gap, the local convective heat transfer value with transient simulation was found almost 20% higher in comparison with the stationary case for e = 0.8. Simulations were carried out under Reynolds number of 7300 and Prandlt 0.71. The flow dynamic of the flow was not affected by the thermal field.

INTRODUCTION

Forced convection heat transfer and the flow characteristics in annulus passages are important phenomena in the engineering field. An eccentric annular duct is a prototype element in a number of engineering applications. Many engineering applications have either concentric or eccentric annulus pipe flow, such as double-pipe heat exchanger, close-packed tubular heat exchangers arranged in a rod bundle, coolant channels of nuclear reactors containing clusters of fuel pins, for instance. Eccentricity in annular passages may appear due to fabrication or construction errors or tolerance, leading to misalignment tube, producing narrow gaps [1]. Turbulent flow and its characteristics deserve to be studied in eccentric channels mainly because it is the ideal model to investigate inhomogeneous turbulent flows, since, according to [2], the turbulence production experiences significant variation within the cross-section. The authors furthered their conclusions pointed out the fact that will be easy to think it as a model to study laminar/turbulent flow interface, since in the narrow gap the local Reynolds drops significantly.

NOMENCLATURE

A	[m²]	Area
e	[-]	Eccentricity, e = 2Δy/(D-d)
Dh	[m]	Hydraulic diameter
d	[m]	Inner Diameter
D	[m]	Outer Diameter
f	[-]	Darcy friction factor
h	[W/m²K]	Convective heat transfer coefficient
k	[W/mK]	Thermal conductivity
L	[m]	Streamwise length of the channel
Nu	[-]	Nusselt number
$q"$	[W/m²]	Heat flux
P	[Pa]	Pressure
Pr	[-]	Prandtl number
Re	[-]	Reynolds number, Re = uDh/ν
T	[K]	Temperature
u	[m/s]	Streamwise velocity component
w	[m/s]	Spanwise velocity component
x	[m]	Cartesian axis direction
y	[m]	Cartesian axis direction
$y+$	[-]	Dimensionless distance from wall
z	[m]	Cartesian axis direction

Special characters

α	[m²/s]	Thermal diffusity
ρ	[Kg/m³]	Density
ν	[m²/s]	Kinematic viscosity
τ	[Pa]	Shear stress
ϕ	[degree]	Angular Coordinate with respect to the rod center

Subscripts

b	Bulk
in	Inlet
s	Surface
T	Turbulent
w	Wall

Both numerical and experimental campaigns have been conducted over the last century in order to raise awareness on the flow field details and/or the process of heat transfer in such kinds of channels. Most of the authors aimed their work to obtain correlations for predicting the heat transfer process, based on the flow regime, Reynolds and Prandtl numbers. [3] were the first authors to produce a Nusselt correlation, so far

well employed in many engineering textbooks and real-life applications.

The Douglas's work [4], is a very early work whose the main scopus was the investigation on the flow field in concentric and eccentric annulus. The work aimed to understand how eccentricity can affect the flow field. The author carried out experimental measurements with Reynolds number ranging from 20000 to 55000 and eccentricities varying from 0%, 50% and 100%. After the measurements, the author drew some conclusions: a) for all eccentricities, the friction factor obeyed a general rule, $f=CRe^{-m}$, where C and m were constants and functions of the eccentricity, Re is the Reynolds number. b) in case of 100% eccentric annulus, f was found 20% higher in comparison with the concentric one. c) in regard with the intermediate eccentric annulus, the friction factor yielded was less affected by the eccentricity. Further, the author fitted f -data using almost the same coefficients (C and m) used in the Blasius's equation. The local shear stress distribution around the inner tube was also a target of research by the author. The dimensionless wall shear ($\tau_w / \overline{\tau_w}$) produced different distributions for eccentricity 50% and 100%. For the first one the highest value was seen at the wider gap, whereas for the second eccentricity the highest value was found at 40° (in his work ϕ = 0º is aligned with the wider gap). The author explained both effects through the velocity gradient near the inner tube's wall. For the 100% eccentricity the gradient was steeper between 40° < ϕ < 60°, whereas for the intermediated case the velocity gradient was smoother near by the narrow gap (ϕ = 180°).

One of the most remarkable characteristics in channels whose the flow pass through a narrow passage, as in the case of the annulus with high eccentricity, are the high turbulence intensity at the narrow gap vicinity, the high cross flux through the gap [1, 2, 5, 6, 7, 8, 9]. In these works, the authors are very sure that cross-motion flow are the truly responsible for the mixing process enhancement at the gap vicinity. [10] used velocity and temperature probes to investigate a heated 37-rod bumbles disposed in triangular array at different p/d-ratios (1.12 and 1.06). Through the time-history velocity measurements, the authors identified peaks in the spectra indicating the presence of large scales for p/d = 1.06. As regards the temperature, no matter what p/d-ratio was studied the highest value was found in the narrow gap, indicating the lowest heat transfer convection. Also, they concluded that the turbulent quantities, the turbulent intensities, turbulent kinetic energy and the temperature fluctuation are similar that found in pipes when p/d-ratio is 1.12. The opposite was found for the lowest gap (p/d = 1.06) where the time traces velocities showed quasi-periodic patterns.

In the present paper, both steady-state and time-dependent simulations were performed to describe the mean average and time-dependent fields in a non-isothermal turbulent flow inside an annulus. Throughout the computations, the Reynolds number (based on the entrance velocity, u_{bulk}, the hydraulic-diameter, D_h, and the kinematic viscosity, v), the Prandtl number were kept constant, as well as the thermal boundary conditions and the d/D-ratio and domain's length. The Reynolds number was calculated as 7300, the Prandtl number was 0.71. At the inner wall heat flux was imposed as q'' = 1000 [W/m²] and the inlet temperature was kept 25 [°C]. Finally, to perform stationary computations we chose k-ω SST model whilst the time-dependent solutions were predicted by URANS/LES Hybrid model, DES.

MESH AND DOMAIN

In this paper, non-isothermal turbulent flow behaviour was simulated in a concentric and eccentric annulus, d/D = 0.494. Air was chosen as work fluid, with its physical properties at the room temperature. Three different simulations were run for two eccentricities, e = 0 (concentric case) and 0.8, being 2 of them under stationary and 1 under time-dependent regime.

The geometry was designed to perfectly match its geometrical characteristics with that previously published by [1], shown in Figure 1. The inner and outer tubes are 25.10 and 50.80 mm, respectively, yielding a L/Dh - ratio about 58.36.

At the entrance, a bulk velocity, temperature and a turbulence intensity was imposed, by following, as much as possible, the previous work [1]. The velocity was imposed null at the walls. Concerning the thermal boundary conditions at the inner and outer walls, a heat flux of q'' = 1000 [W/m²], was prescribed at the first one, whereas in the outer wall an adiabatic condition was imposed.

The physical properties of the work fluid (air) were set up at the beginning of the computations and were kept unchanged as the bulk temperature rises and the flow develops along the annulus. By these settings, both Reynolds and Prandtl numbers were constant throughout the computations, being 7300 and 0.71, respectively. The Reynolds number was based on the bulk velocity, the hydraulic-diameter and the kinematic viscosity, whereas the Prandtl number deals with the ratio between momentum and thermal diffusivity, v/α.

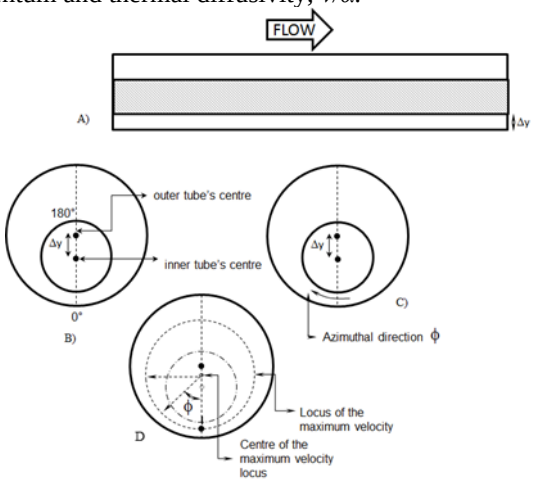

Figure 1 Sketch of the eccentric annulus [1]

The eccentricity was done by displacing the center of the inner tube from the center of the outer one by a distance Δy.

Mesh Validation

For the eccentric case simulation, the work mesh had the same number of nodes used by [1]. However, for the concentric domain up to 2.4-million-element mesh was produced to test them.

Different meshes were tested before reaching the working mesh. The tests were focused on the $y+$ values near the walls, the pressure drop factor, f, and the mean average Nusselt number, since there are analytical correlations to describe such quantities [11].

In order to identify how the results are sensitivity to the mesh, it was conducted a refinement about 50 percent in four meshes for concentric annulus. Both, the pressure drop factor, f, and the mean average Nusselt number were predicted through stationary simulations and k-ω SST as a function of the meshes. All tested meshes presented $y+$ lower than one. Table 1 shows the main parameters of the tested meshes and the quantities observed.

Table 1 Darcy friction factor and Nusselt number.

Mesh	Million of nodes	$f=\frac{\Delta P}{\frac{1}{2}\rho U_b^2}\frac{D_h}{L}$	$Nu=\frac{hD_h}{k}$	No. of divisions in x-axis
M1	0.3	0.1106	27.28	100
M2	0.6	0.0369	27.45	100
M3	1.2	0.0366	27.01	120
M4	2.4	0.0372	27.01	120

With exception of M1, all of them presented similar results in terms of mean average Nusselt number the friction factor. In this regard, due to the time consuming generated by a heavy mesh, we decided to use the mesh M3 for the concentric case.

GOVERNING EQUATIONS AND TURBULENCE MODEL

Numerical computations were performed in a commercial Finite Volumes Software ANSYS/CFX, discretizing the domain into small volumes as already mentioned before. The Newtonian incompressible flow field is ruled by the mass conservation and linear momentum balance, as follow:

$$\frac{\partial \overline{u_i}}{\partial x_i}=0 \tag{1}$$

$$\frac{\partial \overline{u}}{\partial t}+\frac{\partial\left(\overline{u_i u_j}\right)}{\partial x_j}=-\frac{1}{\overline{\rho}}\frac{\partial \overline{P}}{\partial x_i}+\nu\frac{\partial^2 \overline{u_i}}{\partial x_j \partial x_j}+\frac{\partial \tau_{ij}}{\partial x_j}$$
$$\tau_{ij}=-\rho\overline{u_i' u_j'}=\mu_T\left(\frac{\partial \overline{u_i}}{\partial x_j}-\frac{\partial \overline{u_j}}{\partial x_i}\right)-\frac{2}{3}\delta_{ij}k \tag{2}$$

The overbars on the equations, depending on the zones where the flow is simulated. Whenever the RANS mode is turned on the overbar means that the variable is averaged in time. Further, the turbulent viscosity, μ_T, is computed through the turbulent kinetic energy, k, and the dissipation rate, ω, fields.

On the other hand, in the case where the LES modelling is activated the overbar means that the quantities are filtered in space, based on the grid size. Thus, the Reynolds Stress Tensor is then divided into solved and unsolved parts, being the last one modelled as Sub Grid Scale (SGS). For further details, the reader can see in [1].

RESULTS AND DISCUSSION

Temperature and Nusselt distribution for stationary simulation

In the next paragraphs, the temperature distribution, the convective heat transfer coefficient, mean and local Nusselt number will be stressed and discussed for each stationary case. However, in order to qualify our simulations, we first discuss the k-ω SST and DES results for concentric annulus, facing the analytical expressions achieved by Gnielinski in his work [11]. Applying Gnielinski's correlations both quantities f and the average Nusselt number could be calculated as shown in Table 2.

Table 2 Comparison between simulated flow quantities and the Gnielinski's correlations [11].

Turbulence Model	Time-dependent?	f	Nu	Reynolds and Prandtl
k-ω SST	No	0.0366	27.01	7300 0.71
DES	Yes	0.0367	27.05	
Gnielinski (2009)	-	0.0378	22.24	

As we can see, both simulations have attained good predictions in terms of friction factor. However, for the average Nusselt number the results are a little bit farther in comparison with the correlation proposed by [11].

The local temperature, convective heat transfer coefficient and local Nusselt number are shown as a function of the angular position, ϕ on the inner tube's wall for all the simulated cases. All quantities, related to the inner wall, were gathered at the station x/D_h = 54.50 (at about 1400 mm downstream from the channel's inlet). The temperature, the convective heat transfer and the Nusselt number distribution are stressed according to equation (3), respectively.

$$T=\frac{T_{w(\phi)}-T_{in}}{T_{in}};\quad h=\frac{h_{(\phi)}}{\overline{h}};\quad Nu=\frac{Nu_{(\phi)}}{\overline{Nu}} \tag{3}$$

where $T_w(\phi)$, $h(\phi)$ and $Nu(\phi)$ are the local thermal quantities. The Nusselt number is computed using local convective heat transfer coefficient, $h(\phi)$, the hydraulic-diameter and the fluid thermal conductivity ($Nu(\phi) = h(\phi)\, Dh/k$). The convective heat transfer coefficient is computed through the heat flux imposed to the inner wall, q'' = 1000 [W/m²], the local temperature and the bulk temperature, T_b, by equation (4) [12].

$$h_{(\phi)}=\frac{q''}{\left(T_{w\phi}-T_{Bulk}\right)};\quad T_{Bulk}=\frac{1}{U_{Bulk}A}\int_A U_{Bulk}AT_{(A)}dA \tag{4}$$

In Figure 2, the quantities mentioned above are shown. In the first case, e = 0, there is nothing different from our expectations. All discussed variables were seen unchanged along the inner wall. The convective coefficient was calculated about 27.50 [W/m²K], yielding a Nusselt number 27.05, as shown in Table 2.

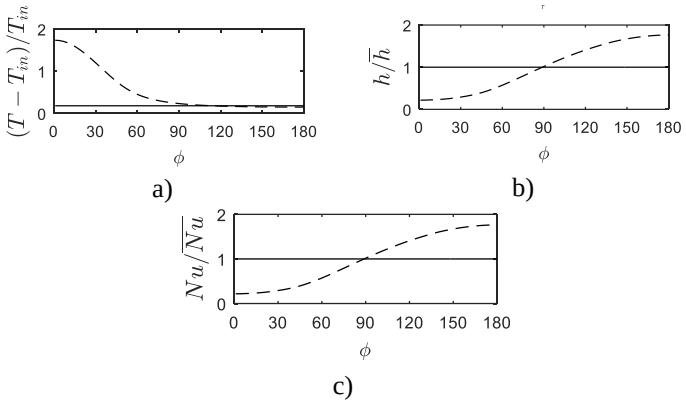

Figure 2 Flow quantities distributed on the inner wall tube: a) Temperature, b) Variation of the convective heat transfer coefficient and c) Nusselt number for concentric case (-) and eccentric case (--)

With regards the eccentric annulus, we have reached a different configuration in terms of variable distribution. All quantities showed different values from the 0° up to 180° (where 0° is in the narrow gap). The wall temperature at the narrow gap increases as the eccentricity becomes higher, producing a contrary effect on the convective heat transfer coefficient, h, whose value is lowered as the eccentricity increases. By observing the results, it is possible to see that the wall temperature, for the eccentric case (e = 0.8), is 9 times higher at the gap in comparison with the first concentric case. The average convective heat transfer coefficient for concentric case is seen to drop from 27 [W/m²K] to 17.15 [W/m²K], as function of the new eccentricity.

TIME-DEPENDENT SIMULATIONS

In this part of the work, the results of the time dependent solutions are going to be presented. In this regard, only results for eccentric case, e = 0.8, will be stressed, since this annulus was the only that showed velocity fluctuations compatible with those ones observed in Candela's work [1].

Temperature field

In Figures 3 and 4, the mean average temperature field is shown. Both stationary and time-dependent results are presented and the temperature is dimensionless according to the equation (3). Comparing both simulations, it is noteworthy that the higher temperatures are stressed in the first case. At the narrow gap vicinity, for instance, the temperature for the stationary case reaches up to 1.7, whereas in the time-dependent solution the thermal field stress about 0.1, at the same location.

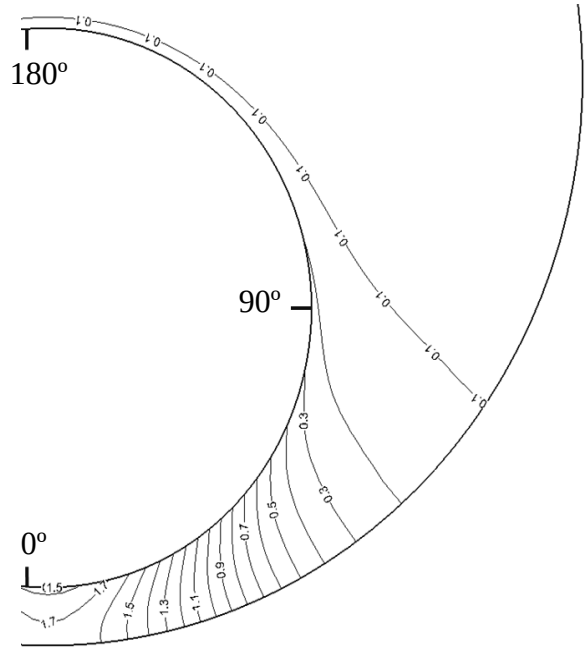

Figure 3 Mean average temperature field for e = 0.8 obtained with stationary simulation

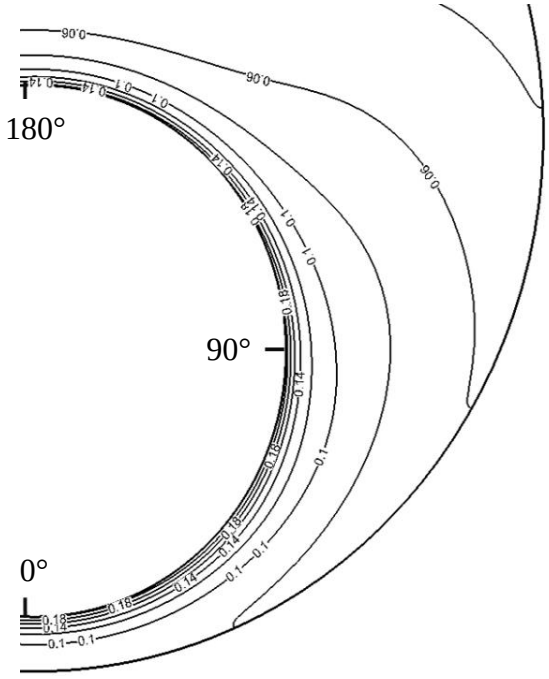

Figure 4 Mean average temperature field for e = 0.8 obtained with time-dependent simulation

Some authors [1, 8, 13, 14] showed in their papers that the flow in annulus passage is prone to instabilities generating large scale motion in the narrow gap. Furthermore, such large vortices promote the flow acceleration inside the gap as they arise, beyond the fact that they are responsible for a mass crossing flux between adjacent subchannel. Surely such movement will cause enhancement in terms forced convection.

In fact, Figure 4 shows the mean average temperature around the inner tube as the distance from the inlet increases. The mean average temperature was calculated from the equation (5) [15,16].

$$\overline{T_{w(x)}} = \frac{1}{2\pi}\int_0^{2\pi} T_{w(x,\phi)} d\phi \quad (5)$$

Only for purpose of comparison all simulated cases are depicted in Figure 5. Let us turn our focus on the stationary and time-dependent cases for the case with e = 0.8. Both simulations showed that the time average temperature around the inner wall departure from the same value. In case of stationary simulation, the temperature rises until the channel's outlet. On the other hand, the time-dependent run was able to capture the velocity fluctuations, as shown by [1, 13].

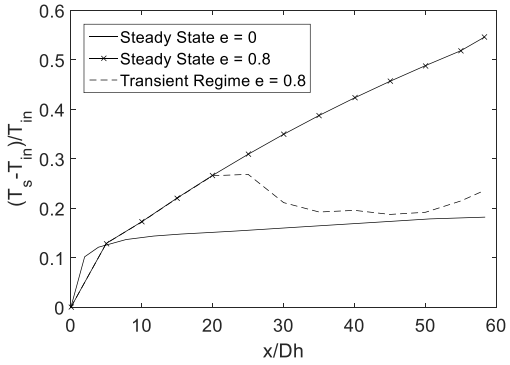

Figure 5 Rod surface temperature along the channel for different eccentricities for stationary and transient regime.

The oscillating flow starts at about x/D_h ~ 20, as shown in Figure 6. Just at this position, both stationary and time dependent simulations detaches from each other. In the case of transient solution, the inner wall average temperature drops reaching values quite similar from those ones simulated for the concentric case. In Figure 6b, the reader can also observe the high crossflow component, w'/u_{bulk}, that starts to cross the narrow, with an amplitude of about 30% of the bulk velocity. As regards the mean axial velocity in the narrow gap, u/u_{bulk}, it is noteworthy to mention that the flow velocity increasing from very marginal value up to almost 60% of the bulk velocity (Figure 6a), at the time of the onset gap instability.

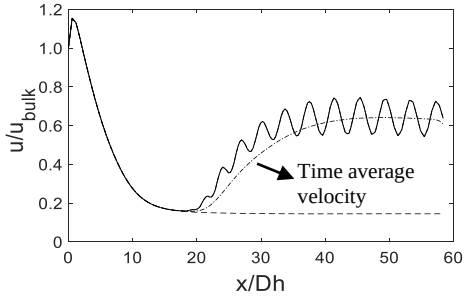

a)

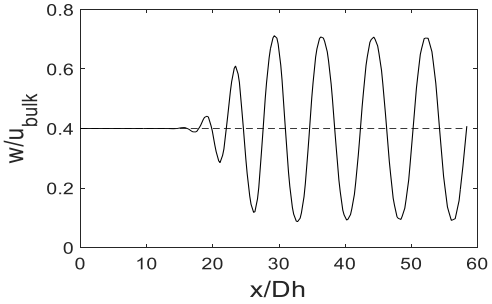

b)

Figure 6 a) Mean axial velocity and b) Spanwise crossflow component. (-) Instantaneous velocity and (--) Stationary simulation velocity

In this scenario, the mean average Nusselt numbers is certainly modified in comparison with that one computed in the stationary case. Figure 7 shows the Nusselt number distribution on the inner wall's surface for both transient and stationary cases, along with the temperature distribution.

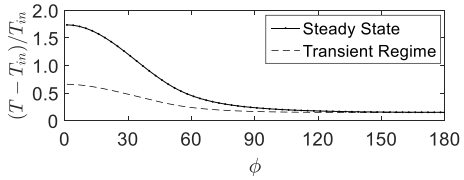

a)

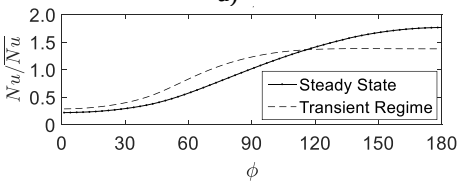

b)

Figure 7 a) Local Temperature and b) Nusselt distribution on the inner wall's surface

As regards the Nusselt number, it was seen that its value is enhanced in the narrow gap in comparison with the stationary case. In the stationary case, its value is $Nu_{(\phi)}/\overline{Nu}$ = 0.20, facing the transient simulation that whose value was found 0.30. The gap wall temperature is also seen to lower from T-T_{in}/T_{in} = 1.80 for the stationary case to one-thirty of this value, reaching 0.6 for the transient simulation.

CONCLUSION

In the present study, a concentric and an eccentric annulus were simulated with the same boundary conditions in order to compare the thermal behavior around the inner tube. Three simulation were performed, two for the steady state regime and one transient run with the eccentric case. The friction factor calculated for the concentric case agreed with the open literature [11]. Also, comparing concentric and eccentric results, we saw that the eccentric case reported an increase at wall temperatures. The contrary happened with the convective heat transfer coefficient as the eccentricity increased. For the time-dependent simulations with e = 0.8, it was seen

fluctuations at the transient run which improved the heat transfer phenomena at the gap. To support this found, the rod surface temperature for steady state and transient runs showed the same growth path until $x/D_h \sim 20$, where the oscillations started. After this point, the inner wall average temperature slipped and reached values close to the ones found in concentric case. The local Nusselt number at the inner wall was also affected by the presence of fluctuations, but the average value kept unchanged for eccentric case e = 0.8.

REFERENCES

[1] Candela, D. S., Gomes, T. F., Goulart, J. N. V., & Anflor, C. T. M. (2020). Numerical simulation of turbulent flow in an eccentric channel. *European Journal of Mechanics-B/Fluids*, 83, 86-98.

[2] Nikitin, N. V., Chernyshenko, S. I., & Wang, H. L. (2009). Turbulent flow and heat transfer in eccentric annulus. In *Advances in Turbulence XII* (pp. 601-604). Springer, Berlin, Heidelberg.

[3] Dittus, F. W., & Boelter, L. M. K. (1930). University of California publications on engineering. *University of California publications in Engineering*, 2, 371.

[4] Denton, J. D. (1963). Turbulent flow in concentric and eccentric annuli (Doctoral dissertation, University of British Columbia).

[5] Goulart, J. N., Anflor, C., & Möller, S. V. (2013). Static and dynamic characteristics of turbulent flow in a closed compound channel. *Revista Facultad de Ingeniería Universidad de Antioquia*, (68), 124-135.

[6] Goulart, J., Wissink, J. G., & Wrobel, L. C. (2016). Numerical simulation of turbulent flow in a channel containing a small slot. *International Journal of Heat and Fluid Flow*, 61, 343-354.

[7] de Melo, T., Goulart, J. N., Anflor, C. T., & dos Santos, E. (2017). Experimental investigation of the velocity time-traces of the turbulent flow in a rectangular channel with a lateral slot. *European Journal of Mechanics-B/Fluids*, 62, 130-138.

[8] Piot, E., & Tavoularis, S. (2011). Gap instability of laminar flows in eccentric annular channels. *Nuclear engineering and design*, 241(11), 4615-4620.

[9] Chang, D., & Tavoularis, S. (2012). Numerical simulations of developing flow and vortex street in a rectangular channel with a cylindrical core. *Nuclear Engineering and Design*, 243, 176-199.

[10] Krauss, T., & Meyer, L. (1998). Experimental investigation of turbulent transport of momentum and energy in a heated rod bundle. *Nuclear Engineering and design*, 180(3), 185-206.

[11] Gnielinski, V. (2009). Heat transfer coefficients for turbulent flow in concentric annular ducts. *Heat transfer engineering*, 30(6), 431-436.

[12] Bejan, A., & Kraus, A. D. (Eds.). (2003). Heat transfer handbook (Vol. 1). *John Wiley & Sons*.

[13] Choueiri, G., & Tavoularis, S. (2014). Flow instability and vortex street in eccentric annular channels. In *APS Division of Fluid Dynamics Meeting Abstracts* (pp. D12-009).

[14] Merzari, E., Wang, S., Ninokata, H., & Theofilis, V. (2008). Biglobal linear stability analysis for the flow in eccentric annular channels and a related geometry. Physics of Fluids, 20(11), 114104.

[15] Chang, D., & Tavoularis, S. (2007). Numerical simulation of turbulent flow in a 37-rod bundle. *Nuclear Engineering and Design*, 237(6), 575-590.

[16] Chang, D., & Tavoularis, S. (2008). Simulations of turbulence, heat transfer and mixing across narrow gaps between rod-bundle subchannels. *Nuclear Engineering and Design*, 238(1), 109-123.